

# Macrocyclic Octapeptide Binding and Inferences on Protein Substrate Binding to Histone Deacetylase 6

Paris R. Watson, Suchetana Gupta, Parisa Hosseinzadeh, Benjamin P. Brown, David Baker, and David W. Christianson\*



Cite This: <https://doi.org/10.1021/acscchembio.3c00113>



Read Online

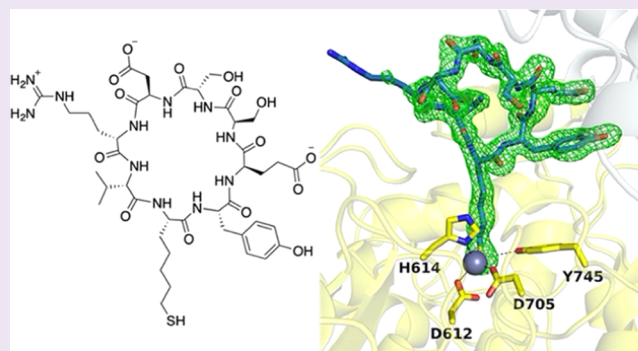
ACCESS |

Metrics & More

Article Recommendations

Supporting Information

**ABSTRACT:** Histone deacetylases (HDACs) are essential for the regulation of myriad biological processes, and their aberrant function is implicated in cancer, neurodegeneration, and other diseases. The cytosolic isozyme HDAC6 is unique among the greater family of deacetylases in that it contains two catalytic domains, CD1 and CD2. HDAC6 CD2 is responsible for tubulin deacetylase and tau deacetylase activities, inhibition of which is a key goal as new therapeutic approaches are explored. Of particular interest as HDAC inhibitors are naturally occurring cyclic tetrapeptides such as Trapoxin A or HC Toxin, or the cyclic depsipeptides Largazole and Romidepsin. Even more intriguing are larger, computationally designed macrocyclic peptide inhibitors. Here, we report the 2.0 Å resolution crystal structure of HDAC6 CD2 complexed with macrocyclic octapeptide 1. Comparison with the previously reported structure of the complex with macrocyclic octapeptide 2 reveals that a potent thiolate–zinc interaction made by the unnatural amino acid (*S*)-2-amino-7-sulfanylheptanoic acid contributes to nanomolar inhibitory potency for each inhibitor. Apart from this zinc-binding residue, octapeptides adopt strikingly different overall conformations and make few direct hydrogen bonds with the protein. Intermolecular interactions are dominated by water-mediated hydrogen bonds; in essence, water molecules appear to cushion the enzyme–octapeptide interface. In view of the broad specificity observed for protein substrates of HDAC6 CD2, we suggest that the binding of macrocyclic octapeptides may mimic certain features of the binding of macromolecular protein substrates.



## INTRODUCTION

Reversible posttranslational modifications allow for the regulation of protein function and myriad cellular processes,<sup>1,2</sup> and lysine residues in particular are subject to a variety of such modifications, including acetylation.<sup>3</sup> At physiological pH, the side chain of lysine is positively charged; neutralization of this charge by acetylation can influence interactions with binding partners.<sup>4</sup> Two key enzyme families govern lysine acetylation: lysine acetyltransferases and lysine deacetylases, the latter family also known as histone deacetylases (HDACs). The HDACs consist of 18 enzymes divided into four classes based on phylogenetic analysis.<sup>5</sup> The zinc-dependent HDACs adopt the arginase-deacetylase fold and consist of class I (HDACs 1–3 and 8), class IIa (HDACs 4,5,7,9), class IIb (HDACs 6 and 10; HDAC6 contains two catalytic domains, CD1 and CD2), and class IV (HDAC11) deacetylases.<sup>6,7</sup> The class III enzymes, better known as sirtuins, adopt a different fold and employ an alternative chemical mechanism for lysine deacetylation.<sup>8,9</sup> The history of HDAC nomenclature is based on Allfrey's discovery of histone acetylation nearly 60 years ago,<sup>10</sup> but this nomenclature belies the diversity of this enzyme family: HDACs differ in expression patterns, cellular localization, and

catalytic activities. Moreover, HDAC substrates include more than just histone proteins, since proteomics studies indicate that 5–10% of mammalian proteins are subject to lysine acetylation.<sup>11–13</sup> Additionally, there is catalytic diversity even within the HDAC family in that HDAC10 is a polyamine deacetylase<sup>14</sup> and HDAC11 is a lysine fatty-acid deacylase.<sup>15,16</sup>

Inhibition of HDAC isozymes represents a critical thrust in medicinal chemistry due to the link between aberrant HDAC activity and human diseases. Currently, four HDAC inhibitors have been approved for clinical use by the U.S. Food and Drug Administration (FDA).<sup>17,18</sup> The general design of HDAC inhibitors consists of three components: a zinc-binding group, a hydrophobic linker, and a capping group that can interact with the outer active site surface.<sup>19</sup> A fascinating group of HDAC inhibitors includes cyclic peptide or depsipeptide

Received: February 22, 2023

Accepted: March 31, 2023

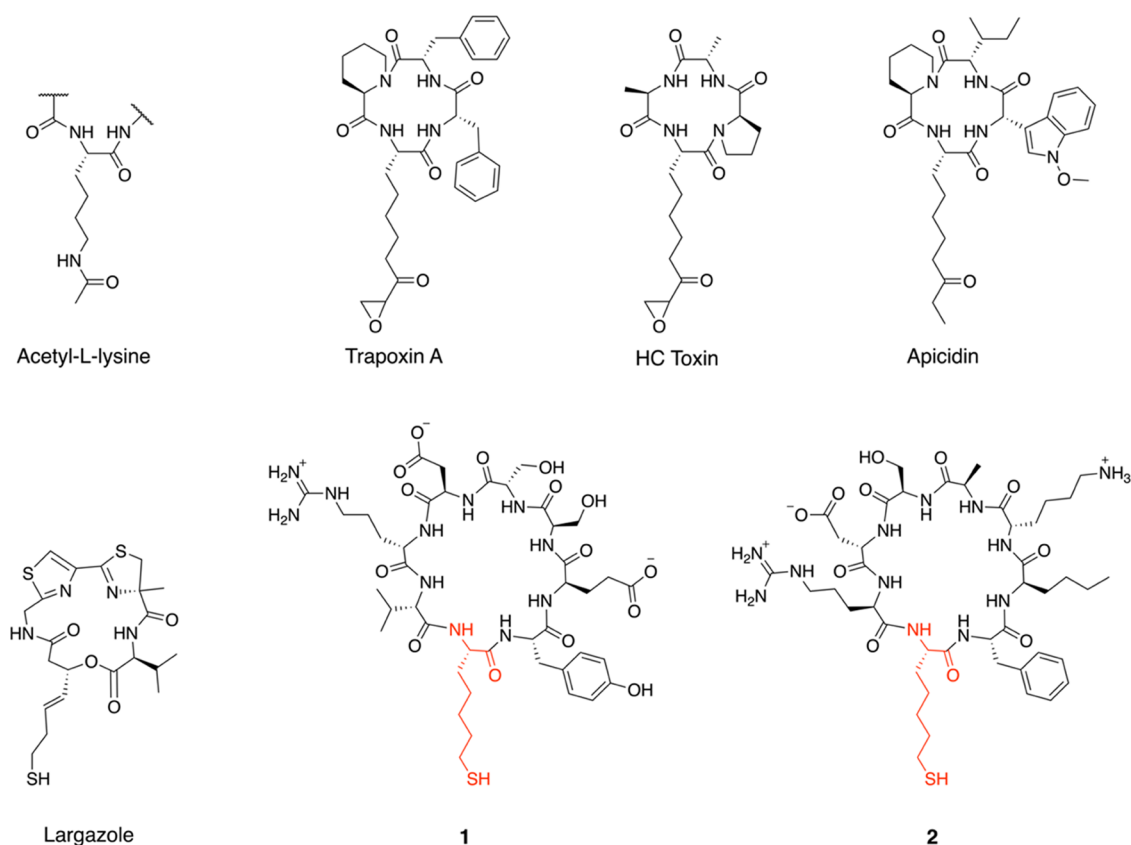


**Figure 1.** Comparison of the HDAC substrate acetyllysine with macrocyclic peptide and depsipeptide inhibitors. Cyclic peptide natural products Trapoxin A, HC Toxin, and Apicidin contain epoxyketone or ketone side chains in which the ketone carbonyl is isosteric with the amide carbonyl of acetyllysine. The ketone carbonyl undergoes nucleophilic attack by zinc-bound solvent to yield a zinc-bound gem-diol(ate) that mimics the tetrahedral intermediate in acetyllysine hydrolysis. The cyclic depsipeptide natural product Largazole thiol and the *de novo* designed macrocyclic peptides 1 ( $IC_{50} = 4.4$  nM) and 2 ( $IC_{50} = 3.6$  nM) contain thiol side chains that target zinc coordination. The zinc-binding residue, (S)-2-amino-7-sulfanylheptanoic acid (SHA), is highlighted in red in 1 and 2. The  $IC_{50}$  = 670 nM for pure SHA, so interactions with the remainder of each macrocyclic octapeptide enhance the inhibitory activity by more than 150-fold.<sup>37</sup>

natural products, which can differ in the structures of their zinc-binding groups and their macrocyclic capping groups (Figure 1). Such macrocyclic inhibitors have been isolated from various sources including fungi, cyanobacteria, proteobacteria, and marine invertebrates.<sup>20,21</sup>

The cyclic tetrapeptide inhibitors Trapoxin A and HC Toxin contain epoxyketone zinc-binding groups. Crystal structures of the HDAC8–Trapoxin A and HDAC6 CD2–HC Toxin complexes reveal that the ketone group of each inhibitor undergoes nucleophilic attack by a zinc-bound solvent to form a gem-diolate (thus mimicking the tetrahedral intermediate in the HDAC mechanism).<sup>22,23</sup> The epoxide moiety of each inhibitor is not required for gem-diolate formation, since the ketone group of Apicidin similarly binds to HDAC2 as a gem-diolate.<sup>24</sup> Ketones readily undergo nucleophilic attack by the metal-bound solvent in zinc hydrolase active sites to yield gem-diolates, as first demonstrated with carboxypeptidase A.<sup>25,26</sup>

In contrast, Largazole thiol is a cyclic depsipeptide with a thiolate zinc-binding group liberated by hydrolysis of a thioester precursor.<sup>27,28</sup> The crystal structure of the HDAC8–Largazole thiol complex shows that the inhibitor side chain thiolate group coordinates to the catalytic zinc ion with nearly perfect geometry.<sup>29</sup> The macrocyclic backbone of Largazole thiol partially mimics that of the reduced, active form of Romidepsin, a cyclic depsipeptide approved by the FDA for the treatment of cutaneous T-cell lymphoma.<sup>30,31</sup>

Cyclic peptides can mimic structural features of proteins including loops, strands, helices, and turns.<sup>32,33</sup> Elements of such mimicry are evident in the binding of the cyclic tetrapeptides HC Toxin and Trapoxin A to HDAC6 CD2 and HDAC8, respectively, since the conformation of the zinc-binding residue is generally identical to that of the acetyllysine substrate in complexes with these HDACs.<sup>22,23,34</sup> Thus, a zinc-binding residue in a cyclic peptide as small as a tetrapeptide can still adopt an ideal conformation for binding in an HDAC active site. With regard to the potential for structure-based drug design, the rigidity of cyclic peptides can enhance metabolic stability, binding affinity, and target specificity.<sup>35,36</sup> Thus, there is significant potential for the development of selective high-affinity cyclic peptides that inhibit HDAC isozymes.

Recently, a computational approach termed “anchor extension” was developed in which macrocyclic peptides containing eight or nine amino acids were optimized for binding to the active site of HDAC2.<sup>37</sup> During the course of this investigation, selective high-affinity inhibitors of HDAC6 CD2 were discovered. HDAC6 CD2 is a tubulin deacetylase,<sup>38,39</sup> inhibition of which leads to cell cycle arrest and apoptosis, which makes this isozyme an attractive target for cancer chemotherapy.<sup>40,41</sup> HDAC6 CD2 is also a tau deacetylase,<sup>42,43</sup> and its inhibition may accordingly be useful in the treatment of neurodegenerative disorders.<sup>44,45</sup> Thus, the

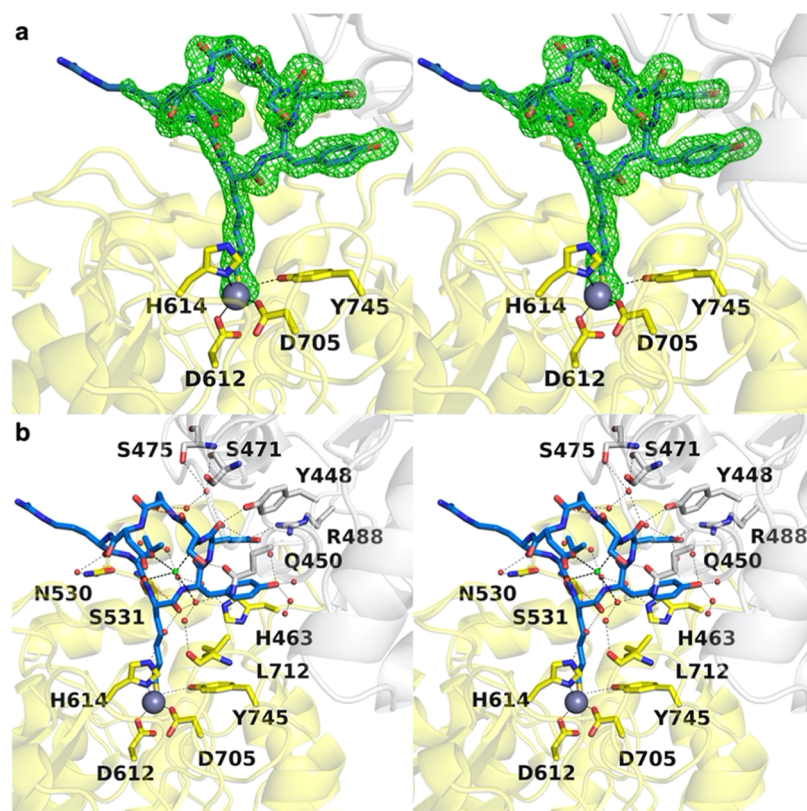


**Figure 2.** Crystal structure of the HDAC6 CD2–1 complex. Atomic color codes are as follows: C = yellow (chain B), gray (chain A), or blue (inhibitor 1); N = blue; O = red; and S = yellow. (a) Polder omit map of inhibitor 1 (contoured at  $3.0\sigma$ ). (b) Hydrogen bond interactions (dashed black lines),  $n \rightarrow \pi^*$  interactions (dashed orange lines), and metal coordination interactions (solid black lines). The catalytic  $\text{Zn}^{2+}$  ion is shown as a gray sphere and water molecules are shown as red spheres. The water molecule in the center of the macrocycle that makes three hydrogen bond interactions with the peptide backbone and a fourth hydrogen bond with another water molecule is shown as a green sphere.

pharmaceutical importance of HDAC6 CD2 drives the discovery of new inhibitor designs and an understanding of their structure–affinity relationships.

Here, we report the 2.0 Å resolution X-ray crystal structure of HDAC6 CD2 complexed with one of these macrocyclic octapeptide inhibitors, originally referred to<sup>37</sup> as “des4.2.0” and here referred to simply as compound 1 (Figure 1). The crystal structure of macrocyclic octapeptide inhibitor “des4.3.1” (compound 2, Figure 1) complexed with HDAC6 CD2 was described in the original report.<sup>37</sup> These cyclic peptides contain an unnatural amino acid side chain, (*S*)-2-amino-7-sulfanylheptanoic acid (SHA), containing a thiol group that coordinates to the catalytic zinc ion. Notably, these are the largest peptides successfully cocrystallized with any HDAC isozyme, and their binding modes provide fascinating inferences on protein–protein recognition. While the conformations of the zinc-bound SHA residues are generally identical for 1 and 2, the macrocyclic octapeptides otherwise adopt strikingly different conformations. The majority of enzyme–inhibitor interactions are water-mediated, which may suggest that a flexible cushion of water molecules in the outer active site cleft facilitates broad specificity while maintaining high affinity. These water-mediated interactions contribute to more than a 150-fold enhancement of inhibitory activity: 1 and 2 exhibit  $\text{IC}_{50}$  values of 4.4 and 3.6 nM, respectively, against HDAC6 CD2, whereas for SHA alone,  $\text{IC}_{50} = 670$  nM.<sup>37</sup> We suggest that the binding of these high-affinity peptide macrocycles may mimic certain features of the binding of high-activity protein substrates.

## RESULTS AND DISCUSSION

**Structure of the HDAC6 CD2–1 Complex.** The X-ray crystal structure of the HDAC6 CD2–1 complex was solved at 2.0 Å resolution. The overall backbone conformation and most side chain conformations of the macrocycle are clearly outlined in the electron density map (Figure 2a); only the solvent-exposed side chain of Arg-7 is characterized by weak or missing density, presumably due to disorder (henceforth, macrocyclic peptide and protein residues are indicated by three- and one-letter amino acid abbreviations, respectively).

Inhibitor binding does not trigger any major structural changes in comparison with the unliganded enzyme, and the root-mean-square deviation (rmsd) is 0.18 Å for 312  $\text{C}\alpha$  atoms between the two structures. The inhibitor makes several intermolecular and intramolecular interactions in the active site (Figure 2b), key among which is coordination of the catalytic  $\text{Zn}^{2+}$  ion by the SHA-1 thiolate group ( $\text{S}\cdots\text{Zn}^{2+}$  separation = 2.3 Å,  $\text{C}-\text{S}\cdots\text{Zn}^{2+}$  angle =  $119^\circ$ , and  $\text{C}-\text{C}-\text{S}\cdots\text{Zn}^{2+}$  dihedral angle =  $32^\circ$ ). The  $\text{Zn}^{2+}$ -bound thiolate also accepts a hydrogen bond from Y745. Apart from the  $\text{C}-\text{C}-\text{S}\cdots\text{Zn}^{2+}$  dihedral angle, thiolate–zinc coordination geometry is generally similar to that observed in the HDAC8–Largazole complex.<sup>29</sup>

The macrocycle makes three additional hydrogen bonds with protein residues, but just one of these interactions is biologically relevant: the backbone NH group of SHA-1 donates a hydrogen bond to the side chain hydroxyl group of S531, just as the backbone NH groups of acetyllysine in two different linear peptide substrates donate hydrogen bonds to S531.<sup>22</sup> This is the only direct interaction made with the

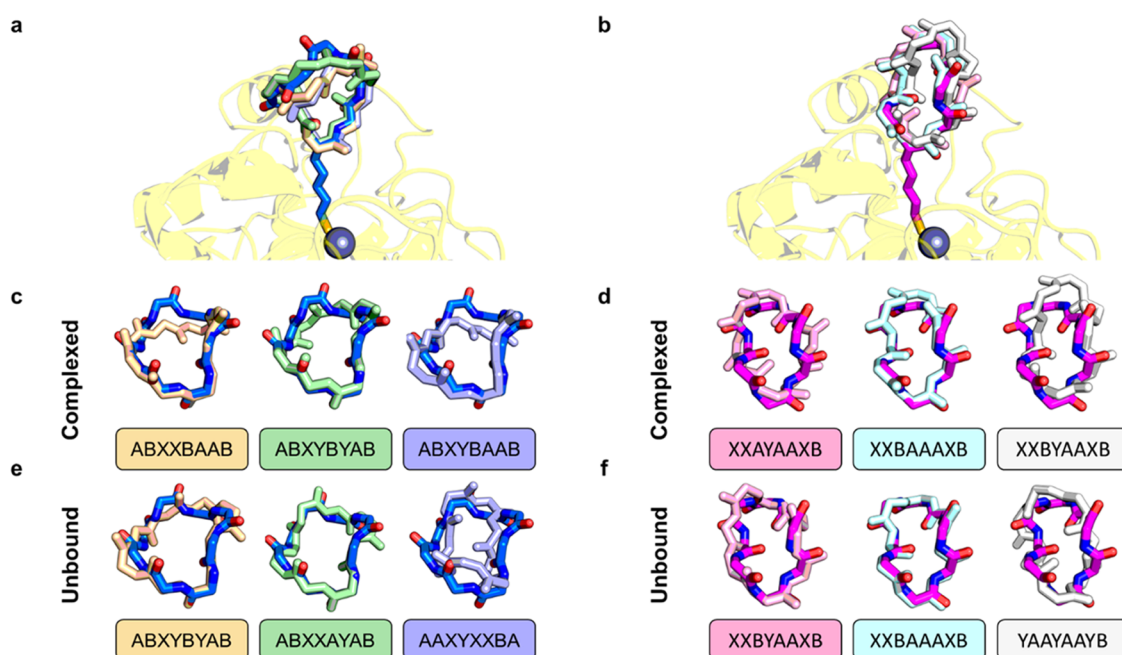


**Figure 3.** Molecular dynamics simulations of **1** and **2** in HDAC6 CD2-bound and unbound states. Superpositions of the crystallographically determined structures of **1** (a) and **2** (b) bound to HDAC6 CD2 are shown with representative structures from the three highest occupancy clusters identified in MD simulations of the complexes. Each representative MD structure is shown in pairwise comparison with the crystallographically determined structures of **1** (c) and **2** (d). Torsion angle bins for clusters A–C and X–Z are defined in Table S1. Each individual unbound peptide MD simulation cluster representative is compared with the crystallographically determined structure of **1** (e) or **2** (f). A total of 110  $\mu$ s of MD simulations were performed (10 independent trials of the unbound peptide for 5  $\mu$ s each for each peptide and five independent trials of the HDAC6 CD2–peptide complex for 1  $\mu$ s each for each peptide). Simulation frames were collected every 10 ps.

backbone of the macrocyclic octapeptide, just as it is the only direct interaction made with the backbones of linear peptide substrates. The binding of the macrocyclic octapeptide thus mimics substrate binding.

The remaining two enzyme–inhibitor hydrogen bonds are made with an adjacent HDAC6 CD2 monomer in the crystal lattice. These interactions are not biologically relevant for inhibitory activity since they are the consequence of packing in the crystal lattice: the backbone carbonyl group of dGlu-3 accepts a hydrogen bond from the phenolic hydroxyl group of Y448 in the adjacent monomer, and the side chain hydroxyl group of dSer-4 forms a hydrogen bond with Q450 in the adjacent monomer. It could be argued that interlattice contacts influence the macrocycle conformation, so we utilized molecular dynamics simulations to ascertain the conformational flexibility of **1** as described in the next section.

Other than the intermolecular interactions of SHA-1, the macrocyclic octapeptide makes no direct hydrogen bonds with the protein. However, numerous water-mediated protein–peptide interactions are observed such that the inhibitor appears to sit on a cushion of water molecules (Figure 2b). These water-mediated hydrogen bonds appear to stabilize the peptide conformation; indeed, a single water molecule in the center of the macrocycle forms hydrogen bonds with the side chain of dAsp-6, the backbone carbonyl of Val-8, the backbone NH group of dSer-4, and a second water molecule.

Finally, two intramolecular  $n \rightarrow \pi^*$  interactions are observed that may contribute to the stabilization of peptide conformation. The first  $n \rightarrow \pi^*$  interaction occurs between the backbone carbonyl oxygen of Val-8 and the carbonyl carbon of SHA-1, and the second  $n \rightarrow \pi^*$  interaction occurs between the carbonyl oxygen of dSer-4 and the carbonyl carbon of Ser-5 (Figure 2b). Both of these interactions occur

between the  $n$  and  $n + 1$  residues, as also found for  $n \rightarrow \pi^*$  interactions in  $\alpha$ -helices.<sup>46,47</sup> This is notable since the  $\Phi$  and  $\Psi$  angles of SHA-1 correspond to those of a residue in an  $\alpha$ -helix.

**Molecular Dynamics Simulations.** To evaluate the extent to which interlattice contacts influenced the binding conformation of inhibitor **1**, we performed molecular dynamics (MD) simulations of both the free macrocycle as well as its complex with HDAC6 CD2. Given that macrocyclic octapeptide inhibitor **2** (Figure 1) also makes an array of different interlattice contacts (Figure S1), we also performed MD simulations for **2** in both the free and HDAC6 CD2-bound states. In total, we performed 10 independent trials of 5  $\mu$ s each for each unbound macrocyclic octapeptide and five independent trials of 1  $\mu$ s each for each HDAC6 CD2-bound macrocyclic octapeptide.

For each set of simulations, we systematically clustered the trajectories based on backbone dihedral torsion angles in an approach similar to that previously employed for the computational design and analysis of ordered peptide macrocycles.<sup>48</sup> Here, torsion angle bins A–C and X–Z for the analysis of peptide conformations are defined in Table S1 and used in Figure 3 to summarize the MD results.

The top three clusters identified from simulations of either **1** or **2** bound to HDAC6 CD2 account for the majority of the conformational heterogeneity (Figure S2). Each of these clusters preserves the geometry of the zinc-bound SHA residue and adjacent residues with torsional fluctuations primarily in the solvent-exposed region (Figures 3a–d and S2). Notably, simulations of the unbound peptide structures also display substantial preorganization of the SHA residue and adjacent residues for binding to HDAC6 CD2 (Figures 3e,f and S2). Preorganization of key binding site interaction residues in HCDC3 loop-derived macrocyclic peptides was previously

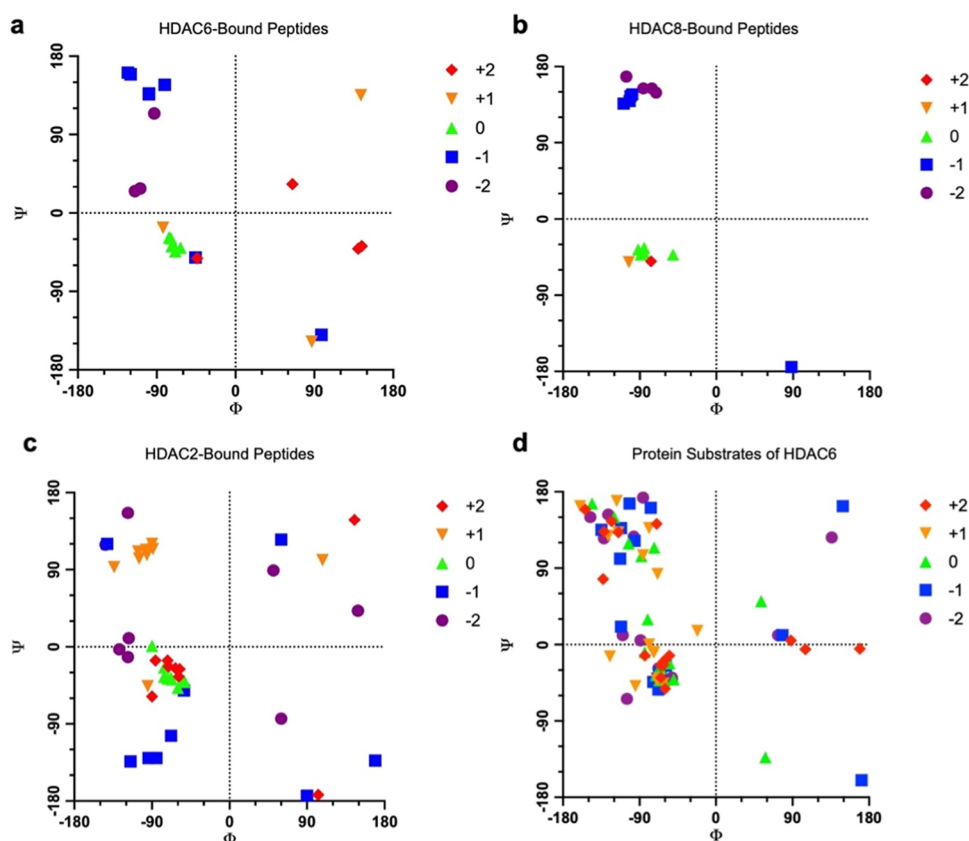


**Figure 4.** (a–c) Ramachandran plots illustrating the conformations of residues flanking acetyllysine or other zinc-binding groups (“residue 0”) in crystal structures of peptide complexes with HDAC isozymes (individual entries are listed in Tables S2–S4). (d) Ramachandran plot illustrating the conformations of residues flanking known lysine acetylation sites in crystal structures of protein substrates of HDAC6 CD2 (individual entries are listed in Tables S5 and S6).

identified as an important contributor to peptide affinity.<sup>49</sup> Similarly, the tertiary structures of the macrocyclic peptides remain near their crystallographic conformers in both simulations of the complexed and unbound states. Altogether, our MD simulation results suggest that interlattice contacts do not appreciably influence the binding poses of the peptide macrocycles to HDAC6 CD2. Specifically, these results indicate that interlattice contacts do not influence or alter binding interactions of the cyclic octapeptide in the HDAC6 CD2 active site.

**Comparison of Enzyme-Bound Inhibitor Conformations.** There are notable differences in the binding conformations of **1** and **2** in the HDAC6 CD2 active site. However, both retain the  $n \rightarrow \pi^*$  interaction between the carbonyl oxygen of residue 8 (Val-8 in **1**, dArg-8 in **2**) and the carbonyl carbon of SHA-1. This interaction, as well as the hydrogen bond between the backbone NH group of SHA-1 in each inhibitor and S531, stabilize the backbone conformation of the zinc-binding residue. Each SHA-1 residue exhibits backbone torsion angles  $\Phi \sim -75^\circ$  and  $\Psi \sim -35^\circ$  comparable to those of zinc-binding residues in all other peptides bound to HDAC6 CD2, HDAC8, or HDAC2, including zinc-bound acetyllysine in linear peptide substrates and zinc-bound epoxyketone or ketone side chains of cyclic tetrapeptide inhibitors (Figure 4a–c and Tables S2–S4 and Figure S3). Regardless of the zinc-binding residue and regardless of its context in a cyclic or linear peptide, its binding conformation is essentially identical in each HDAC active site.

An additional conformational regularity in the peptide backbone is observed for the  $-1$  residue relative to the zinc-binding residue in peptide substrates and inhibitors: apart from the  $-1$  residue in cyclic octapeptide **2** and the cyclic tetrapeptides HC Toxin and Trapoxin A, the  $-1$  residue in complexes with HDAC6 CD2 and HDAC8 adopts backbone torsion angles  $\Phi$  and  $\Psi$  that generally correspond to an extended  $\beta$ -strand conformation (Figure 4a,b and Tables S2 and S3). Less regularity in the conformation of the  $-1$  residue is observed for peptide binding to HDAC2, but here the conformations of the  $+1$  residue tend to cluster in the  $\beta$ -strand region of the Ramachandran plot (Figure 4c and Table S4). A structural trend thus begins to emerge for the conformations of residues immediately flanking the scissile acetyllysine residue that may favor binding to one HDAC isozyme or another.

Beyond the immediate vicinity of the zinc-binding residue, the conformations of macrocyclic octapeptides differ significantly (Figure 5 and Table S2). In its complex with HDAC6 CD2, **2** contains a  $\beta$ -turn in which the backbone carbonyl of Lys-4 accepts a hydrogen bond from the backbone NH group of Asp-7. In comparison, **1** lacks this secondary structural motif and adopts an alternative backbone conformation. Interestingly, two direct intramolecular hydrogen bonds stabilize the macrocyclic peptide conformation in the HDAC6 CD2–**2** complex. In contrast, intramolecular hydrogen bonds are not direct in the HDAC6 CD2–**1** complex but instead are mediated through a central hydrogen-bonded water molecule (Figure 2b).

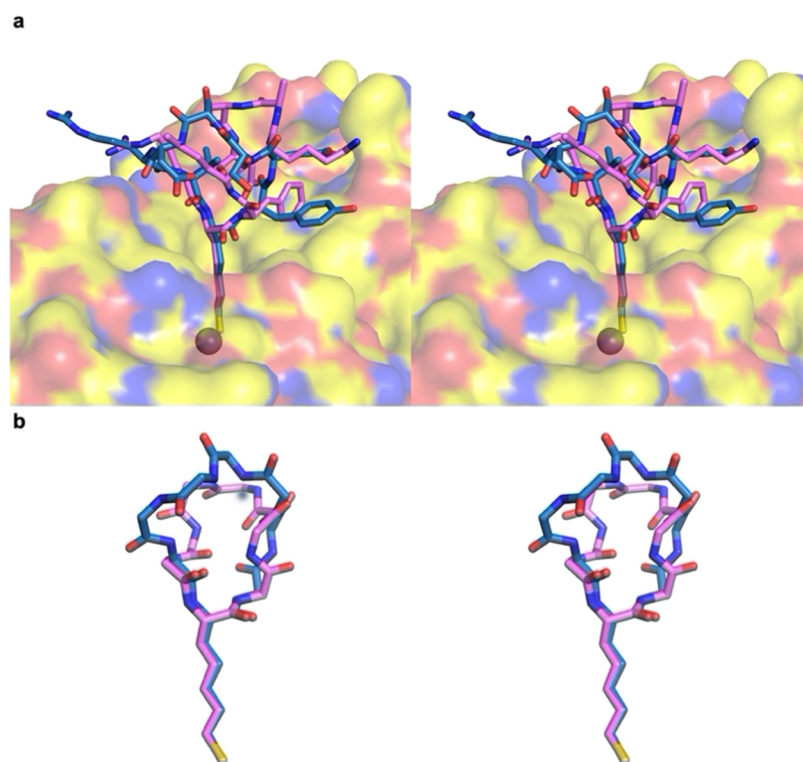


**Figure 5.** (a) Overlay of **1** and **2** (PDB 6WSJ) bound in the active site of HDAC6 CD2. Atomic color coding is as follows: C = blue (**1**), lavender (**2**), or yellow (protein surface); N = dark blue; O = red; and S = dark yellow. (b) Stereoview of the binding conformations of **1** and **2** shown with no side chains except for SHA-1 highlights striking differences in main-chain conformations.

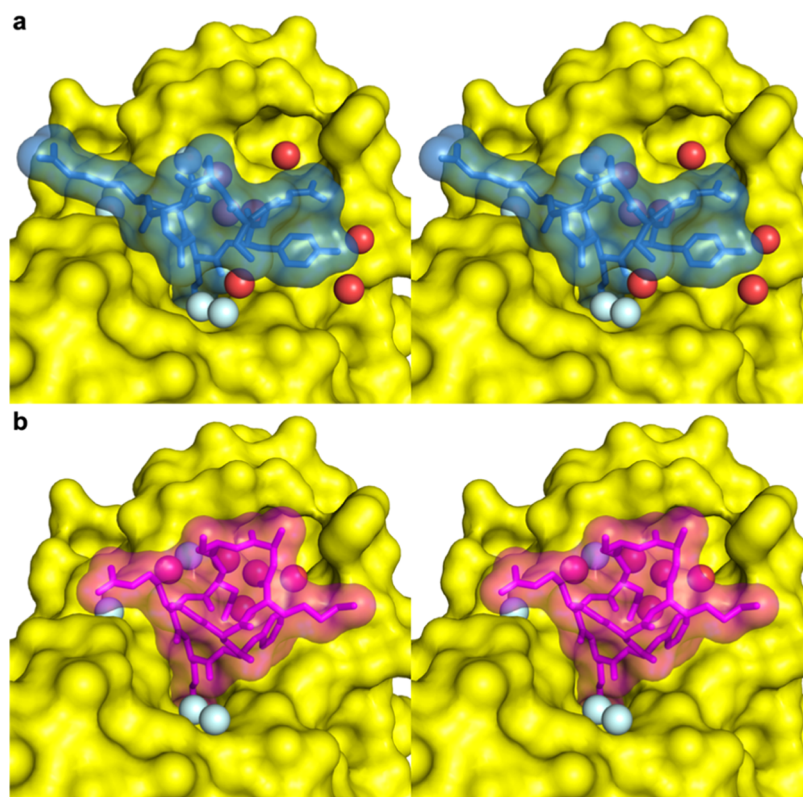


**Figure 6.** Structures of HDAC6 CD2 complexes with **1** (a) and **2** (b) showing molecular surfaces. While the conformations of the SHA-1 residue in each inhibitor are essentially identical, differences in the overall macrocycle conformation yield significant differences in the overall molecular shape. Despite these differences, there is general complementarity of molecular surfaces in the regions where protein–peptide association is closest, especially as mediated by a flexible cushion of water molecules (red spheres). Water molecules common to both structures appear as cyan spheres.

Given that the backbone conformation of SHA-1 in both macrocyclic octapeptides is similar to the backbone conformation of an acetyllysine peptide substrate, we suggest that each macrocyclic octapeptide inhibitor may mimic certain features of the binding of a macromolecular protein substrate in the HDAC6 CD2 active site. Protein–peptide or protein–protein binding requires molecular surfaces with complementary shapes; it is interesting that despite differences in the overall peptide sequence and conformation between **1** and **2**, each inhibitor is generally complementary in shape to the active site contour of HDAC6 CD2. Moreover, the structural complementarity of each inhibitor is facilitated by a cushion of ordered water molecules. Four of these water molecules are conserved in each complex, and the remaining water molecules occupy different positions (Figure 6). It is notable that the active site solvent structure can adjust to accommodate different macrocyclic octapeptides with different conformations yet comparable inhibitory potencies.

**Conformations of Protein Substrates.** Analysis of backbone torsion angles in confirmed protein substrates of HDAC6 CD2 for which structures are available in the Protein Data Bank reveals that many lysine residues known to be reversibly acetylated adopt backbone torsion angles  $\Phi$  and  $\Psi$  characteristic of residues in an  $\alpha$ -helix (Table S5). However, other conformations are also observed, such as  $\beta$ -strand or random coil (loop). Regardless that these lysine residues are known to be HDAC6 CD2 substrates indicates that their conformations must be sufficiently flexible to fit in the active site such that the scissile acetyllysine residue can adopt backbone torsion angles of  $\Phi \sim -75^\circ$  and  $\Psi \sim -35^\circ$ .

In addition to protein substrates of HDAC6 CD2 identified through *in vivo* biochemical methods (Table S5), additional putative protein substrates have been identified by screening peptide fragments *in vitro* for activity and then correlating peptide sequences with the corresponding proteins for which crystal structures are available.<sup>50,51</sup> Analysis of protein structures identified through this approach yields additional examples of lysine residues contained in loops,  $\alpha$ -helices, and one in a  $\beta$ -strand (Table S6).

Conformational analysis of confirmed and putative protein substrates indicates that no trends are evident for the backbone conformations of the substrate acetyllysine residue  $\pm 2$  flanking residues (Figure 4d). This is consistent with the general lack of trends observed for binding conformations of smaller peptides in complexes with HDAC6 CD2, HDAC8, and HDAC2, apart from the conformation of the zinc-binding residue (Figure 4a–c). This conformational variability is consistent with the generally broad substrate specificity of HDAC isozymes. In particular, there is no strong consensus sequence flanking the scissile acetyllysine residue in confirmed and putative protein substrates of HDAC6 CD2 (Figure 7), regardless of whether their structures have been determined (Tables S5 and S6) or not (Tables S7 and S8). As long as the scissile acetyllysine residue can adopt backbone torsion angles of  $\Phi \sim -75^\circ$  and  $\Psi \sim -35^\circ$ , and as long as the backbone torsion angles of flanking residues are sufficiently flexible to enable binding in the active site without causing steric clashes, the acetyllysine residue can be an HDAC substrate. Even if the acetyllysine residue is contained in an  $\alpha$ -helix, the helix does not necessarily have to fully unwind to enable substrate binding in the HDAC6 CD2 active site (Figure S4). However, the ability for the peptide segment to fit in the HDAC6 CD2 active site is necessary but not sufficient for protein substrate binding. Additional

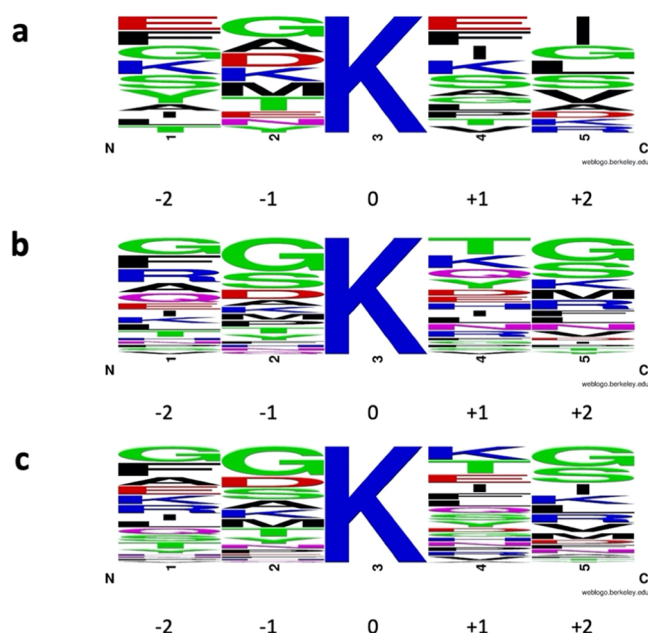


**Figure 7.** Analysis of protein substrates of HDAC6 CD2 reveals no significant consensus sequence flanking the acetyllysine substrate. (a) WebLogo of substrates and putative substrates with known three-dimensional structures as listed in Tables S5 and S6, respectively. (b) WebLogo of substrates and putative substrates for which three-dimensional structures are unavailable, as listed in Tables S7 and S8, respectively. (c) WebLogo resulting from combining sequences in panels (a) and (b).

structural features beyond the scissile acetyllysine residue must be important for molecular recognition of specific HDAC6 CD2 substrates. In other words, if virtually any sequence can fit in the HDAC6 CD2 active site, HDAC6 CD2-substrate recognition must be based in large part on the tertiary structure surrounding the scissile acetyllysine residue and long-range enzyme–substrate interactions.

The importance of long-range interactions for HDAC-substrate recognition and catalysis was first demonstrated for the class I deacetylase HDAC8 using linear peptide substrates.<sup>52</sup> These studies revealed that an exosite accommodates the basic sequence KRHR in the +4 to the +7 position relative to the scissile acetyllysine of peptide substrates and that these distal residues are important for substrate binding and catalysis. More recently, Fierke and colleagues measured steady-state kinetics using singly acetylated histone protein H3 prepared by unnatural amino acid mutagenesis, demonstrating that HDAC8 catalyzes the deacetylation of H3(Ac)/H4 tetramers more efficiently than the deacetylation of the corresponding 7-, 13-, and 17-mer linear peptides.<sup>53</sup> Thus, long-range enzyme–substrate interactions are important for HDAC8 activity with protein substrates. We expect that the same holds true for HDAC6 CD2 activity with protein substrates.

## CONCLUSIONS

The X-ray crystal structure of the HDAC6 CD2–**1** complex reveals that a potent thiolate–zinc interaction made by SHA-1, also stabilized by a hydrogen bond with Y745, contributes to nanomolar inhibitory potency. The macrocyclic octapeptide makes only one additional direct interaction with the protein: the backbone NH group of SHA-1 donates a hydrogen bond to

the hydroxyl group of S531, thereby mimicking the hydrogen bond interaction made by the acetyllysine residue of an actual HDAC6 CD2 substrate.<sup>22</sup> All other hydrogen bond interactions between the enzyme and the macrocyclic octapeptide by residues flanking SHA-1 are made through intervening water molecules. Peptide binding is accommodated by a cushion of water molecules in the outer active site cleft.

Similar conclusions hold for the previously reported<sup>37</sup> crystal structure of the HDAC6 CD2–2 complex, *i.e.*, no direct enzyme–inhibitor hydrogen bonds are observed apart from interactions with SHA-1, and inhibitor binding is accommodated by a cushion of water molecules. Macrocyclic polypeptides 1 and 2 adopt strikingly different conformations apart from the SHA-1 residue when bound to HDAC6 CD2, yet each conformation exploits shape complementarity for binding in the enzyme active site with nanomolar inhibitory potency. Thus, high-affinity binding of a macrocyclic peptide inhibitor is based on molecular recognition of the tertiary structure rather than the primary structure surrounding the zinc-binding residue and may be facilitated by a flexible cushion of water molecules. We suggest that the same conclusion may hold for the binding of protein substrates to HDAC6 CD2. This feature may contribute to the broad protein substrate specificity of HDAC6 CD2 as well as other lysine deacetylases in the HDAC family.

## METHODS

For X-ray crystallography, catalytic domain 2 from *Danio rerio* (HDAC6 CD2) encoded in the His<sub>6</sub>-MBP-TEV-HDAC6-pET28a(+) vector was purified as previously described.<sup>54</sup> Macrocyclic octapeptide inhibitor 1 (des4.2.0) was prepared as described.<sup>57</sup> The HDAC6 CD2–1 complex was crystallized *via* sitting drop vapor diffusion and full details of the structure determination at 2.0 Å resolution are summarized in the [Supporting Information](#).

For sequence analyses of protein substrates, WebLogos were generated using the online server at <https://weblogo.berkeley.edu>.<sup>55,56</sup>

For computational modeling, we performed refinement of both the crystallographically solved protein–peptide complexes and the peptides in the unbound state using Rosetta. Following refinement in Rosetta, we prepared our models for all-atom explicit solvent molecular dynamics (MD) simulations in Amber.<sup>57</sup> A total of 10 independent simulations were run for 5.0  $\mu$ s each for each of the unbound peptides. A total of five independent simulations were run for 1.0  $\mu$ s each for each of the HDAC-bound peptides. Altogether, the total production simulation time was therefore 110  $\mu$ s. We analyzed our simulation trajectories through torsion-based clustering. A detailed description of our molecular modeling protocols is found in the [Supporting Information](#).

## ASSOCIATED CONTENT

### Supporting Information

The Supporting Information is available free of charge at <https://pubs.acs.org/doi/10.1021/acscchembio.3c00113>.

Complete methods for X-ray crystallography and molecular dynamics simulations; torsion angle bins (Table S1); torsion angles of peptides bound to HDAC isozymes (Tables S2–S4); backbone torsion angles of HDAC6 CD2 substrates (Table S5); backbone torsion angles of putative HDAC6 CD2 substrates (Table S6); protein substrates of HDAC6 CD2 with unknown structures (Table S7); putative protein substrates of HDAC6 CD2 with unknown structures (Table S8); X-ray data collection and refinement

statistics (Table S9); stereoview of the HDAC6 CD2–2 complex (Figure S1); conformational clusters in MD simulations (Figure S2); binding conformations of macrocyclic octapeptide 1, cyclic tetrapeptide HC Toxin, and a linear peptide substrate (Figure S3); and docking of  $\alpha$ -helices in the HDAC6 CD2 active site (Figure S4) ([PDF](#))

## Accession Codes

Atomic coordinates and structure factor amplitudes of the HDAC6 CD2–1 complex have been deposited in the Protein Data Bank ([www.rcsb.org](http://www.rcsb.org)) with accession code 8EQI.

## AUTHOR INFORMATION

### Corresponding Author

David W. Christianson – Roy and Diana Vagelos Laboratories, Department of Chemistry, University of Pennsylvania, Philadelphia, Pennsylvania 19104-6323, United States; [orcid.org/0000-0002-0194-5212](https://orcid.org/0000-0002-0194-5212); Email: [chris@sas.upenn.edu](mailto:chris@sas.upenn.edu)

### Authors

Paris R. Watson – Roy and Diana Vagelos Laboratories, Department of Chemistry, University of Pennsylvania, Philadelphia, Pennsylvania 19104-6323, United States

Suchetana Gupta – Department of Bioengineering, Knight Campus, University of Oregon, Eugene, Oregon 97403, United States

Parisa Hosseinzadeh – Department of Bioengineering, Knight Campus, University of Oregon, Eugene, Oregon 97403, United States; [orcid.org/0000-0002-3128-7433](https://orcid.org/0000-0002-3128-7433)

Benjamin P. Brown – Department of Chemistry, Center for Structural Biology, Vanderbilt University, Nashville, Tennessee 37235, United States; [orcid.org/0000-0001-5296-087X](https://orcid.org/0000-0001-5296-087X)

David Baker – Department of Biochemistry, Institute for Protein Design, University of Washington, Seattle, Washington 98195, United States

Complete contact information is available at: <https://pubs.acs.org/doi/10.1021/acscchembio.3c00113>

### Funding

This research was supported by NIH Grant GM49758 (D.W.C.). P.H. was supported by NIH NRSA Grant 5 F32 GM120791-02 and a WRF Innovation Fellows Fellowship. P.H. and S.G. were supported by NIH Grant 1DP2GM146249-01.

### Notes

The authors declare no competing financial interest.

## ACKNOWLEDGMENTS

This work is based on research conducted at beamline 17-ID-1 (AMX) of the National Synchrotron Light Source II, a DOE Office of Science User Facility operated for the DOE Office of Science by Brookhaven National Laboratory under Contract DE-SC0012704. The Center for BioMolecular Structure (CBMS) is primarily supported by the National Institutes of Health, NIGMS, through a Center Core P30 Grant (P30GM133893) and by the DOE Office of Biological and Environmental Research (KP1605010).

## REFERENCES

- (1) Walsh, C. T.; Garneau-Tsodikova, S.; Gatto, G. J., Jr. Protein posttranslational modifications: the chemistry of proteome diversifications. *Angew. Chem., Int. Ed.* **2005**, *44*, 7342–7372.
- (2) Leutert, M.; Entwisle, S. W.; Villén, J. Decoding post-translational modification crosstalk with proteomics. *Mol. Cell. Proteomics* **2021**, *20*, No. 100129.
- (3) Wang, Z. A.; Cole, P. A. The chemical biology of reversible lysine post-translational modifications. *Cell Chem. Biol.* **2020**, *27*, 953–969.
- (4) Choudhary, C.; Kumar, C.; Gnad, F.; Nielsen, M. L.; Rehman, M.; Walther, T. C.; Olsen, J. V.; Mann, M. Lysine acetylation targets protein complexes and co-regulates major cellular functions. *Science* **2009**, *325*, 834–840.
- (5) Gregoret, I. V.; Lee, Y. M.; Goodson, H. V. Molecular evolution of the histone deacetylase family: functional implications of phylogenetic analysis. *J. Mol. Biol.* **2004**, *338*, 17–31.
- (6) Lombardi, P. M.; Cole, K. E.; Dowling, D. P.; Christianson, D. W. Structure, mechanism, and inhibition of histone deacetylases and related metalloenzymes. *Curr. Opin. Struct. Biol.* **2011**, *21*, 735–743.
- (7) Porter, N. J.; Christianson, D. W. Structure, mechanism, and inhibition of the zinc-dependent histone deacetylases. *Curr. Opin. Struct. Biol.* **2019**, *59*, 9–18.
- (8) Yuan, H.; Marmorstein, R. Structural basis for sirtuin activity and inhibition. *J. Biol. Chem.* **2012**, *287*, 42428–42435.
- (9) Jing, H.; Lin, H. Sirtuins in epigenetic regulation. *Chem. Rev.* **2015**, *115*, 2350–2375.
- (10) Allfrey, V. G.; Faulkner, R.; Mirsky, A. E. Acetylation and methylation of histones and their possible role in the regulation of RNA synthesis. *Proc. Natl. Acad. Sci. U.S.A.* **1964**, *51*, 786–794.
- (11) Haberland, M.; Montgomery, R. L.; Olson, E. N. The many roles of histone deacetylases in development and physiology: implications for disease and therapy. *Nat. Rev. Genet.* **2009**, *10*, 32–42.
- (12) Choudhary, C.; Weinert, B. T.; Nishida, Y.; Verdin, E.; Mann, M. The growing landscape of lysine acetylation links metabolism and cell signalling. *Nat. Rev. Mol. Cell Biol.* **2014**, *15*, 536–550.
- (13) Kim, G. W.; Yang, X. J. Comprehensive lysine acetylomes emerging from bacteria to humans. *Trends Biochem. Sci.* **2011**, *36*, 211–220.
- (14) Hai, Y.; Shinsky, S. A.; Porter, N. J.; Christianson, D. W. Histone deacetylase 10 structure and molecular function as a polyamine deacetylase. *Nat. Commun.* **2017**, *8*, No. 15368.
- (15) Kutil, Z.; Novakova, Z.; Meleshin, M.; Mikesova, J.; Schutkowski, M.; Barinka, C. Histone deacetylase 11 is a fatty-acid deacetylase. *ACS Chem. Biol.* **2018**, *13*, 685–693.
- (16) Moreno-Yruela, C.; Galleano, I.; Madsen, A. S.; Olsen, C. A. Histone deacetylase 11 is an  $\epsilon$ -N-myrystoyllysine hydrolase. *Cell Chem. Biol.* **2018**, *25*, 849–856.
- (17) West, A. C.; Johnstone, R. W. New and emerging HDAC inhibitors for cancer treatment. *J. Clin. Invest.* **2014**, *124*, 30–39.
- (18) Ma, N.; Luo, Y.; Wang, Y.; Liao, C.; Ye, W. C.; Jiang, S. Selective histone deacetylase inhibitors with anticancer activity. *Curr. Top. Med. Chem.* **2015**, *16*, 415–426.
- (19) Osko, J. D.; Christianson, D. W. Structural determinants of affinity and selectivity in the binding of inhibitors to histone deacetylase 6. *Bioorg. Med. Chem. Lett.* **2020**, *30*, No. 127023.
- (20) Maolanon, A. R.; Kristensen, H. M.; Leman, L. J.; Ghadiri, M. R.; Olsen, C. A. Natural and synthetic macrocyclic inhibitors of the histone deacetylase enzymes. *ChemBioChem* **2017**, *18*, 5–49.
- (21) Kitir, B.; Maolanon, A. R.; Ohm, R. G.; Colaço, A. R.; Fristrup, P.; Madsen, A. S.; Olsen, C. A. Chemical editing of macrocyclic natural products and kinetic profiling reveal slow, tight-binding histone deacetylase inhibitors with picomolar affinities. *Biochemistry* **2017**, *56*, 5134–5146.
- (22) Hai, Y.; Christianson, D. W. Histone deacetylase 6 structure and molecular basis of catalysis and inhibition. *Nat. Chem. Biol.* **2016**, *12*, 741–747.
- (23) Porter, N. J.; Christianson, D. W. Binding of the microbial cyclic tetrapeptide Trapoxin A to the class I histone deacetylase HDAC8. *ACS Chem. Biol.* **2017**, *12*, 2281–2286.
- (24) Beshore, D. C.; Adam, G. C.; Barnard, R. J. O.; Burlein, C.; Gallicchio, S. N.; Holloway, M. K.; Krosky, D.; Lemaire, W.; Myers, R. W.; Patel, S.; Plotkin, M. A.; Powell, D. A.; Rada, V.; Cox, C. D.; Coleman, P. J.; Klein, D. J.; Wolkenberg, S. E. Redefining the histone deacetylase inhibitor pharmacophore: high potency with no zinc cofactor interaction. *ACS Med. Chem. Lett.* **2021**, *12*, 540–547.
- (25) Christianson, D. W.; Lipscomb, W. N. Binding of a possible transition state analogue to the active site of carboxypeptidase A. *Proc. Natl. Acad. Sci. U.S.A.* **1985**, *82*, 6840–6844.
- (26) Christianson, D. W.; David, P. R.; Lipscomb, W. N. Mechanism of carboxypeptidase A: hydration of a ketonic substrate analogue. *Proc. Natl. Acad. Sci. U.S.A.* **1987**, *84*, 1512–1515.
- (27) Taori, K.; Paul, V. J.; Luesch, H. Structure and activity of Largazole, a potent antiproliferative agent from the Floridian marine cyanobacterium *Symploca* sp. *J. Am. Chem. Soc.* **2008**, *130*, 1806–1807.
- (28) Ying, Y.; Taori, K.; Kim, H.; Hong, J.; Luesch, H. Total synthesis and molecular target of Largazole, a histone deacetylase inhibitor. *J. Am. Chem. Soc.* **2008**, *130*, 8455–8459.
- (29) Cole, K. E.; Dowling, D. P.; Boone, M. A.; Phillips, A. J.; Christianson, D. W. Structural basis of the antiproliferative activity of Largazole, a depsipeptide inhibitor of the histone deacetylases. *J. Am. Chem. Soc.* **2011**, *133*, 12474–12477.
- (30) Furumai, R.; Matsuyama, A.; Kobashi, N.; Lee, K.-H.; Nishiyama, M.; Nakajima, H.; Tanaka, A.; Komatsu, Y.; Nishino, N.; Yoshida, M.; Horinouchi, S. FK228 (depsipeptide) as a natural prodrug that inhibits class I histone deacetylases. *Cancer Res.* **2002**, *62*, 4916–4921.
- (31) Guan, P.; Fang, H. Clinical development of histone deacetylase inhibitor romidepsin. *Drug Discoveries Ther.* **2010**, *4*, 388–391.
- (32) Hill, T. A.; Shepherd, N. E.; Diness, F.; Fairlie, D. P. Constraining cyclic peptides to mimic protein structure motifs. *Angew. Chem., Int. Ed.* **2014**, *53*, 13020–13041.
- (33) Gavenonis, J.; Sheneman, B. A.; Siegert, T. R.; Eshelman, M. R.; Kritzer, J. A. Comprehensive analysis of loops at protein-protein interfaces for macrocycle design. *Nat. Chem. Biol.* **2014**, *10*, 716–722.
- (34) Dowling, D. P.; Gantt, S. L.; Gattis, S. G.; Fierke, C. A.; Christianson, D. W. Structural studies of human histone deacetylase 8 and its site-specific variants complexed with substrate and inhibitors. *Biochemistry* **2008**, *47*, 13554–13563.
- (35) Huang, H.; Damjanovic, J.; Miao, J.; Lin, Y. S. Cyclic peptides: backbone rigidification and capability of mimicking motifs at protein-protein interfaces. *Phys. Chem. Chem. Phys.* **2021**, *23*, 607–616.
- (36) Jing, X.; Jin, K. A gold mine for drug discovery: Strategies to develop cyclic peptides into therapies. *Med. Res. Rev.* **2020**, *40*, 753–810.
- (37) Hosseinzadeh, P.; Watson, P. R.; Craven, T. W.; Li, X.; Rettie, S.; Pardo-Avila, F.; Bera, A. K.; Mulligan, V. K.; Lu, P.; Ford, A. S.; Weitzner, B. D.; Stewart, L. J.; Moyer, A. P.; Di Piazza, M.; Whalen, J. G.; Greisen, P. J.; Christianson, D. W.; Baker, D. Anchor extension: a structure-guided approach to design cyclic peptides targeting enzyme active sites. *Nat. Commun.* **2021**, *12*, No. 3384.
- (38) Hubbert, C.; Guardiola, A.; Shao, R.; Kawaguchi, Y.; Ito, A.; Nixon, A.; Yoshida, M.; Wang, X. F.; Yao, T. P. HDAC6 is a microtubule-associated deacetylase. *Nature* **2002**, *417*, 455–458.
- (39) Zhang, Y.; Li, N.; Caron, C.; Matthias, G.; Hess, D.; Khochbin, S.; Matthias, P. HDAC-6 interacts with and deacetylates tubulin and microtubules *in vivo*. *EMBO J.* **2003**, *22*, 1168–1179.
- (40) Seidel, C.; Schneckeburger, M.; Dicato, M.; Diederich, M. Histone deacetylase 6 in health and disease. *Epigenomics* **2015**, *7*, 103–118.
- (41) Yang, P. H.; Zhang, L.; Zhang, Y. J.; Zhang, J.; Xu, W. F. HDAC6: physiological function and its selective inhibitors for cancer treatment. *Drug Discoveries Ther.* **2013**, *7*, 233–242.
- (42) Cohen, T. J.; Guo, J. L.; Hurtado, D. E.; Kwong, L. K.; Mills, I. P.; Trojanowski, J. Q.; Lee, V. M. Y. The acetylation of tau inhibits its

function and promotes pathological tau aggregation. *Nat. Commun.* **2011**, *2*, No. 252.

(43) Min, S. W.; Cho, S. H.; Zhou, Y.; Schroeder, S.; Haroutunian, V.; Seeley, W. W.; Huang, E. J.; Shen, Y.; Masliah, E.; Mukherjee, C.; Meyers, D.; Cole, P. A.; Ott, M.; Gan, L. Acetylation of tau inhibits its degradation and contributes to tauopathy. *Neuron* **2010**, *67*, 953–966.

(44) Trübe, O.; Matthias, P. Interplay between histone deacetylases and autophagy – from cancer therapy to neurodegeneration. *Immunol. Cell Biol.* **2012**, *90*, 78–84.

(45) Li, Y.; Lin, S.; Gu, Z.; Chen, L.; He, B. Zinc-dependent deacetylases (HDACs) as potential targets for treating Alzheimer's disease. *Bioorg. Med. Chem. Lett.* **2022**, *76*, No. 129015.

(46) Choudhary, A.; Gandla, D.; Krow, G. R.; Raines, R. T. Nature of amide carbonyl-carbonyl interactions in proteins. *J. Am. Chem. Soc.* **2009**, *131*, 7244–7246.

(47) Newberry, R. W.; Raines, R. T. The  $n \rightarrow \pi^*$  interaction. *Acc. Chem. Res.* **2017**, *50*, 1838–1846.

(48) Hosseinzadeh, P.; Bhardwaj, G.; Mulligan, V. K.; et al. Comprehensive computational design of ordered peptide macrocycles. *Science* **2017**, *358*, 1461–1466.

(49) Sevy, A. M.; Gilchuk, I. M.; Brown, B. P.; Bozhanova, N. G.; Nargi, R.; Jensen, M.; Meiler, J.; Crowe, J. E., Jr. Computationally designed cyclic peptides derived from an antibody loop increase breadth of binding for influenza variants. *Structure* **2020**, *28*, 1114–1123.

(50) Kutil, Z.; Skultetyova, L.; Rauh, D.; Meleshin, M.; Snajdr, I.; Novakova, Z.; Mikesova, J.; Pavlicek, J.; Hadzima, M.; Baranova, P.; Havlinova, B.; Majer, P.; Schutkowski, M.; Barinka, C. The unraveling of substrate specificity of histone deacetylase 6 domains using acetylome peptide microarrays and peptide libraries. *FASEB J.* **2019**, *33*, 4035–4045.

(51) Varga, J. K.; Diffley, K.; Leng, K. R. W.; Fierke, C. A.; Schueler-Furman, O. Structure-based prediction of HDAC6 substrates validated by enzymatic assay reveals determinants of promiscuity and detects new potential substrates. *Sci. Rep.* **2022**, *12*, No. 1788.

(52) Gurard-Levin, Z. A.; Mrksich, M. The activity of HDAC8 depends on local and distal sequences of its peptide substrates. *Biochemistry* **2008**, *47*, 6242–6250.

(53) Castañeda, C. A.; Wolfson, N. A.; Leng, K. R.; Kuo, Y.-M.; Andrews, A. J.; Fierke, C. A. HDAC8 substrate selectivity is determined by long- and short-range interactions leading to enhanced reactivity for full-length histone substrates compared with peptides. *J. Biol. Chem.* **2017**, *292*, 21568–21577.

(54) Osko, J. D.; Christianson, D. W. Methods for the expression, purification, and crystallization of histone deacetylase 6-inhibitor complexes. *Methods Enzymol.* **2019**, *626*, 447–474.

(55) Crooks, G. E.; Hon, G.; Chandonia, J. M.; Brenner, S. E. WebLogo: a sequence logo generator. *Genome Res.* **2004**, *14*, 1188–1190.

(56) Schneider, T. D.; Stephens, R. M. Sequence logos: a new way to display consensus sequences. *Nucleic Acids Res.* **1990**, *18*, 6097–6100.

(57) Case, D. A. et al. *AMBER 2020*; University of California: San Francisco, 2020.

## Recommended by ACS

### Probing Ligand Binding Sites on Large Proteins by Nuclear Magnetic Resonance Spectroscopy of Genetically Encoded Non-Canonical Amino Acids

Kasuni B. Ekanayake, Gottfried Otting, et al.

MARCH 15, 2023  
JOURNAL OF MEDICINAL CHEMISTRY

READ 

### Synthetic Multivalent Disulfide-Constrained Peptide Agonists Potentiate Wnt1/ $\beta$ -Catenin Signaling via LRP6 Coreceptor Clustering

Avinash K. Thakur, Rami N. Hannoush, et al.

MARCH 09, 2023  
ACS CHEMICAL BIOLOGY

READ 

### Development of a Cyclic, Cell Penetrating Peptide Compatible with In Vitro Selection Strategies

Nicolas A. Abrigo, Matthew C. T. Hartman, et al.

MARCH 15, 2023  
ACS CHEMICAL BIOLOGY

READ 

### Evaluating Translational Efficiency of Noncanonical Amino Acids to Inform the Design of Druglike Peptide Libraries

Alix I Chan, Christian N. Cunningham, et al.

JANUARY 06, 2023  
ACS CHEMICAL BIOLOGY

READ 

Get More Suggestions >